AGU ADVANCING EARTH AND SPACE SCIENCES

Water Resources Research

RESEARCH ARTICLE
10.1029/2024WR037508

Attributing Urban Evapotranspiration From Eddy-Covariance to Surface Cover: Bottom-Up Versus Top-Down

H. J. Jongen[1,2], S. Vulova[3,4], F. Meier[5], G. J. Steeneveld[2], F. A. Jansen[1], D. Tetzlaff[6,7], B. Kleinschmit[3], N. Haacke[8], and A. J. Teuling[1]

[1]Hydrology and Environmental Hydraulics, Wageningen University, Wageningen, The Netherlands, [2]Meteorology and Air Quality, Wageningen University, Wageningen, The Netherlands, [3]Geoinformation in Environmental Planning Lab, Department of Landscape Architecture and Environmental Planning, Technische Universität Berlin, Berlin, Germany, [4]Department of Environmental Meteorology, Institute for Landscape Architecture and Landscape Planning, University of Kassel, Kassel, Germany, [5]Chair of Climatology, Technische Universität Berlin, Berlin, Germany, [6]Department of Ecohydrology, Leibniz Institute of Freshwater Ecology and Inland Fisheries, Berlin, Germany, [7]Department of Geography, Humboldt University of Berlin, Berlin, Germany, [8]Ecohydrology and Landscape Evaluation, Institute of Ecology, Technical University Berlin, Berlin, Germany

Abstract Evapotranspiration (*ET*) is a key process in the hydrological cycle that can help mitigate urban heat. *ET* depends on the surface cover, as the surface affects the partitioning of precipitation between runoff and evapotranspiration. In urban neighborhoods, this surface cover is highly heterogeneous. The resulting neighborhood-scale *ET* can be observed with eddy-covariance systems. However, these observations represent the signal from wind- and stability-dependent footprints resulting in a continuously changing contribution of surface cover types to the observation. This continuous change prevents quantifying the contribution of the surface cover types to neighborhood *ET* and their hourly dynamics. Here, we disentangle this neighborhood-scale *ET* at two sites in Berlin attributing the patch-scale *ET* dynamics to the four major surface cover types in the footprint: impervious surfaces, low vegetation, high vegetation, and open water. From the bottom-up, we reconstruct neighborhood *ET* based on patch-scale observations and conceptual models. Alternatively, we start top-down and attribute neighborhood *ET* to the surface cover types solving a system of equations for three eddy-covariance systems. Although data requirements for the bottom-up approach are met more frequently, both approaches indicate that vegetation is responsible for more *ET* than proportional to its surface fraction in the footprint related to the large evaporating surface compared to the ground surface. Evaporation from impervious surfaces cannot be neglected, although it is less than from vegetation due to limited water availability. The limited water availability causes impervious surfaces to cease evaporation hours after rainfall, while vegetation and open water sustain *ET* for extended periods.

Plain Language Summary Different types of surfaces, like grass, trees, pavement, and open water, affect how rainwater is divided between evaporation and runoff. In cities with lots of pavement and buildings, more water runs off than in natural areas leaving less water for evaporation. Measurement towers have been observing the evaporation from whole neighborhoods, but separating the effects of different surfaces is hard. In our study, we figure out how much each surface type contributes to evaporation with two methods: one starting from the separate surfaces and rebuilding the neighborhood evaporation, and the other starting with the neighborhood evaporation and breaking it down into evaporation from each surface. Both ways showed that plants evaporate more than proportionally to their surface area, but even built surfaces like pavement evaporate. Our findings confirm that more plants lead to more evaporation, but built surfaces cannot be ignored. This information can help urban planners create cities that manage water better, making cities nicer places to live.

Key Points:

- Neighborhood ET is reconstructed from patch-scale data (bottom-up) and disentangled attributing ET to four surface types (top-down)
- The neighborhood and patch scale are connected through half-hourly-varying eddy-covariance footprints
- ET dynamics after rainfall reveal that water limitation drives differences between surface cover types

Correspondence to:

H. J. Jongen,
harro.jongen@wur.nl

Citation:

Jongen, H. J., Vulova, S., Meier, F., Steeneveld, G. J., Jansen, F. A., Tetzlaff, D., et al. (2024). Attributing urban evapotranspiration from eddy-covariance to surface cover: Bottom-up versus top-down. *Water Resources Research*, *60*, e2024WR037508. https://doi.org/10.1029/2024WR037508

Received 14 MAR 2024
Accepted 20 AUG 2024

Author Contributions:

Conceptualization: H. J. Jongen
Data curation: H. J. Jongen, S. Vulova, F. Meier
Formal analysis: H. J. Jongen
Funding acquisition: H. J. Jongen, G. J. Steeneveld, A. J. Teuling
Investigation: S. Vulova, F. Meier, D. Tetzlaff, B. Kleinschmit, N. Haacke
Methodology: H. J. Jongen, S. Vulova, F. Meier, G. J. Steeneveld, F. A. Jansen, A. J. Teuling
Project administration: H. J. Jongen
Supervision: G. J. Steeneveld, A. J. Teuling
Visualization: H. J. Jongen
Writing – original draft: H. J. Jongen
Writing – review & editing: H. J. Jongen, S. Vulova, F. Meier, G. J. Steeneveld, F. A. Jansen, D. Tetzlaff, B. Kleinschmit, N. Haacke, A. J. Teuling

1. Introduction

How precipitation is partitioned between runoff and evapotranspiration (*ET*) plays an important role in the urban climate and is governed by the surface cover composition (Oke et al., 2017; Paul & Meyer, 2001). In cities, the abundant impervious surfaces prevent infiltration and promote surface runoff leaving less water available for *ET* than pervious areas (Fletcher et al., 2013; Jongen et al., 2022; McGrane, 2016). On the other hand, urban vegetation has the opposite effect increasing *ET* (Gunawardena et al., 2017; Peters et al., 2011). While all vegetation favors *ET* compared to impervious surfaces, an isotope-based study revealed the vegetation type also

affects infiltration and *ET* patterns (Kuhlemann et al., 2021). The composition of the surface cover thus controls the water partitioning and consequently *ET* dynamics.

Promoting green surface covers by planting vegetation over impervious surfaces can increase *ET* using more of the available energy (Wang & Shu, 2020). Like vegetation, open water is suggested to potentially cool its surroundings by evaporation when implemented appropriately (Jacobs et al., 2020; Solcerova et al., 2019), although warming can also occur due to the high thermal inertia (Steeneveld et al., 2014; Theeuwes et al., 2013). The energy needed for the additional *ET* cannot heat the air, which thus reduces temperatures and mitigates heat stress and the associated health risks (Heaviside et al., 2017; Oke, 1982; Ward & Grimmond, 2017). However, how *ET* at the patch level ($\sim 10^1 - 10^2$ m of a single surface cover type, ET_{patch}) translates to the neighborhood scale ($\sim 10^3$ m, $ET_{neighborhood}$) is largely unknown until now. As *ET* is both an energy and water balance flux, we need to quantify how surface cover impacts the partitioning of incoming water fluxes (Bonneau et al., 2018) and how this affects the partitioning on the larger, neighborhood scale. Ultimately, the neighborhood scale is where the effect of the surface cover types on *ET* needs to be understood. In time, this understanding will support the management of the cooling benefits and urban water demands.

At the neighborhood scale, eddy-covariance (EC) systems observe the *ET* of the combined surface cover types in the footprint at a given moment (Feigenwinter et al., 2012). Even though the heterogeneous urban surface results in spatially variable *ET* (Qin et al., 2022), the observed *ET* represents the weighted average flux in the footprint, as the EC systems are typically installed at a height where the heterogeneous surface flux sources are blended (Oke et al., 2017). The footprint varies temporally depending on the observation height, wind speed/direction, and atmospheric stability (Kljun et al., 2015). Previous research demonstrated it is possible to upscale ET_{patch} observations to the neighborhood-scale EC observations weighed by the contribution of a surface cover type to the footprint climatology at a relatively homogeneous urban site (Peters et al., 2011). However, hour-to-hour variation in the footprint contains useful information to quantify the timing of cooling benefits from *ET*. This time-dependent surface information has been applied to improve the model performance of urban $ET_{neighborhood}$ machine learning models (Vulova et al., 2021). Thus, for heterogeneous urban sites, the footprint is crucial information to disentangle $ET_{neighborhood}$ and attribute it to the different surface cover types.

EC footprints can be estimated with a variety of models. Large-eddy simulations (LES) or Lagrangian stochastic particle dispersion models (LPD) fully model the airflow to find the source area (LES: Leclerc et al., 1997; Wang and Davis, 2008; LPD: Kljun et al., 2002; Hsieh et al., 2003; LES and LPD combined: Hellsten et al., 2015; Auvinen et al., 2017). These models are both labor-intensive and computationally expensive, which limits their applicability to relatively short-duration case studies (Vesala et al., 2008). To analyze longer time series, faster footprint models have been developed with an analytical approach relying on the surface-layer theory (e.g., Kormann & Meixner, 2001; Schmid & Oke, 1990; Schuepp et al., 1990). Their validity is restricted to certain turbulence intensities or stratifications. More recently, Kljun et al. (2015) developed a two-dimensional footprint parameterization that takes away these limitations. Their model yields robust results for most boundary layer conditions at any observation height within the surface layer. This model enables the identification of the flux's source area for a long time series with a wide range of atmospheric conditions. Therefore, this model is suitable to study the influence of the changing footprints on $ET_{neighborhood}$.

To study the influence of surface cover on $ET_{neighborhood}$, Peters et al. (2011) have described the seasonal patterns in urban ET_{patch} from major plant-functional types (trees and turf grass). Vegetation and open water were observed with EC systems and sap flow sensors, while impervious surface evaporation was assumed negligible. The two vegetation types explain the majority of $ET_{neighborhood}$ variation. They also found that the surface fraction of a vegetation type is the most important factor determining its contribution to total $ET_{neighborhood}$ underlining the importance of the EC footprint. Other studies challenge their assumption that impervious surface evaporation can be neglected (Chen et al., 2023; Ramamurthy & Bou-Zeid, 2014). Below, we will test the assumption by including evaporation from impervious surfaces. Moreover, while their analysis is focused on the seasonal timescale, we will consider the hourly timescale. The hourly *ET* dynamics play a key role in the urban climate experienced by urban citizens. As a verification, Peters et al. (2011) compared the sum of their observed ET_{patch} against EC observations, in essence reconstructing the $ET_{neighborhood}$ signal from the bottom up.

While the evaporation dynamics from a single surface cover type have been investigated previously, few studies have addressed these issues across a range of surface cover types. These studies show that surface cover types

have very different evaporation dynamics. Four main surface cover types can be distinguished: impervious surface, low vegetation, high vegetation, and open water. Impervious surfaces only evaporate when wet directly after rainfall resulting in highly dynamic evaporation (Wouters et al., 2015). In contrast, vegetation can draw water from the soil sustaining *ET* long after rainfall (Boese et al., 2019; Teuling et al., 2006). Amongst vegetation, differences are seen with higher average *ET* for higher vegetation with its higher leaf area density than for lower vegetation (Gillefalk et al., 2021, 2022; Kuhlemann et al., 2021). Sufficiently deep open water has more constant evaporation given the abundant water and high heat storage capacity that can provide energy in the absence of solar radiation (Jansen et al., 2022). The term *ET* is used for vegetation because it contains the signals from transpiration, interception, and soil evaporation, and for EC-observed *ET* because it contains the combined signal of the present surface cover types including evaporation, transpiration, and anthropogenic fluxes (e.g., combustion and human metabolism). Over impervious and open water surfaces, only evaporation occurs so the term evaporation is used. We hypothesize these behaviors are combined at the neighborhood scale, as observed with EC, dependent on their relative contribution to the surface.

Very few cities have observations of all relevant hydrometeorological states and fluxes across a range of surface cover types. Berlin is a notable exception. In Berlin, meteorological observations are performed as part of two observatories: the Urban Climate Observatory operated by the Chair of Climatology at the Technische Universität Berlin (https://uco.berlin/en, Scherer et al., 2019) and the Steglitz Urban Ecohydrological Observatory from the IGB Leibniz-Institute of Freshwater Ecology and Inland Fisheries (Kuhlemann et al., 2020, 2021). Additionally, campaigns have added to this observation infrastructure, for example, with drone-based observations (Vulova et al., 2019) or with ground-based remote sensing (Zeeman et al., 2023). The elaborate observation infrastructure has resulted in numerous studies focusing on Berlin (e.g., Fenner et al., 2014, 2023; Meier & Scherer, 2012), of which many focused on *ET*. A modeling study applied a physics-based model to study hourly *ET* (Duarte Rocha et al., 2022), which after validation was combined with remotely sensed vegetation characteristics to map *ET* for all of Berlin (Rocha et al., 2022). Vulova et al. (2021) achieved similar modeling skill with machine learning trained on meteorological and remote sensing data. Because of the research infrastructure and the extensive literature, Berlin offers a unique setting to study the link between the surface cover and *ET*.

In this study, we aim to estimate the *ET* contribution of different surface cover types in the footprint profiting from the diverse observations in Berlin. With this, we will show how the footprint varies over time, how *ET* behaves for each surface cover type, the relation between the surface cover and neighborhood *ET*, and the contribution of each surface cover type to neighborhood *ET*. In this paper, the *ET* contribution is always weighted by the footprint. To study the contribution of each surface cover type to *ET*, we take both a bottom-up and a top-down approach to attribute the EC-observed *ET* to the four dominant surface cover types. For the bottom-up approach, we reconstruct the EC signal by summing the estimated *ET* contribution of each surface cover type weighed by its contribution to the footprint. In this approach, the *ET* contribution of each type is estimated with conceptual models and small-scale observations. These patch-scale models and observations can be verified with the EC observations, as the EC footprint is modeled for every observation. The top-down approach is based on a system of equations, in which each equation describes the surface cover composition of one EC system and its resulting flux. The resulting flux can be attributed to the surface cover types by solving the system of equations. We aim to reveal how the surface cover type influences neighborhood *ET* behavior and to indicate how altering surface cover may affect urban climate. Understanding the relationship between urban surface cover and *ET* can inform future climate-resilient urban design.

2. Study Sites

This study examines observations from the capital and largest city of Germany, Berlin, which has a population of 3.7 million spread over 891 km^2 (Amt für Statistik Berlin-Brandenburg, 2019). Situated in the east of Germany, the climate is temperate oceanic (Cfb) (Kottek et al., 2006). The closest weather station from the German Weather Service (DWD, Berlin-Tempelhof) recorded a long-term (1991–2020) mean annual rainfall of 585 mm and mean air temperature of 10.2°C (DWD, 2021b). Here, we study the warm months (April until October) of the relatively dry year of 2019 with 492 mm of precipitation, in which an intense observation campaign was organized (Vulova et al., 2019). The warm months are studied as most *ET* occurs during this time.

Two sites in Berlin are studied here: a suburban one and one close to the city center. The first, suburban site is an urban research garden located in the southwest of the city at the Rothenburgstraße (ROTH, 52.457°N, 13.315°E,

10.1029/2024WR037508

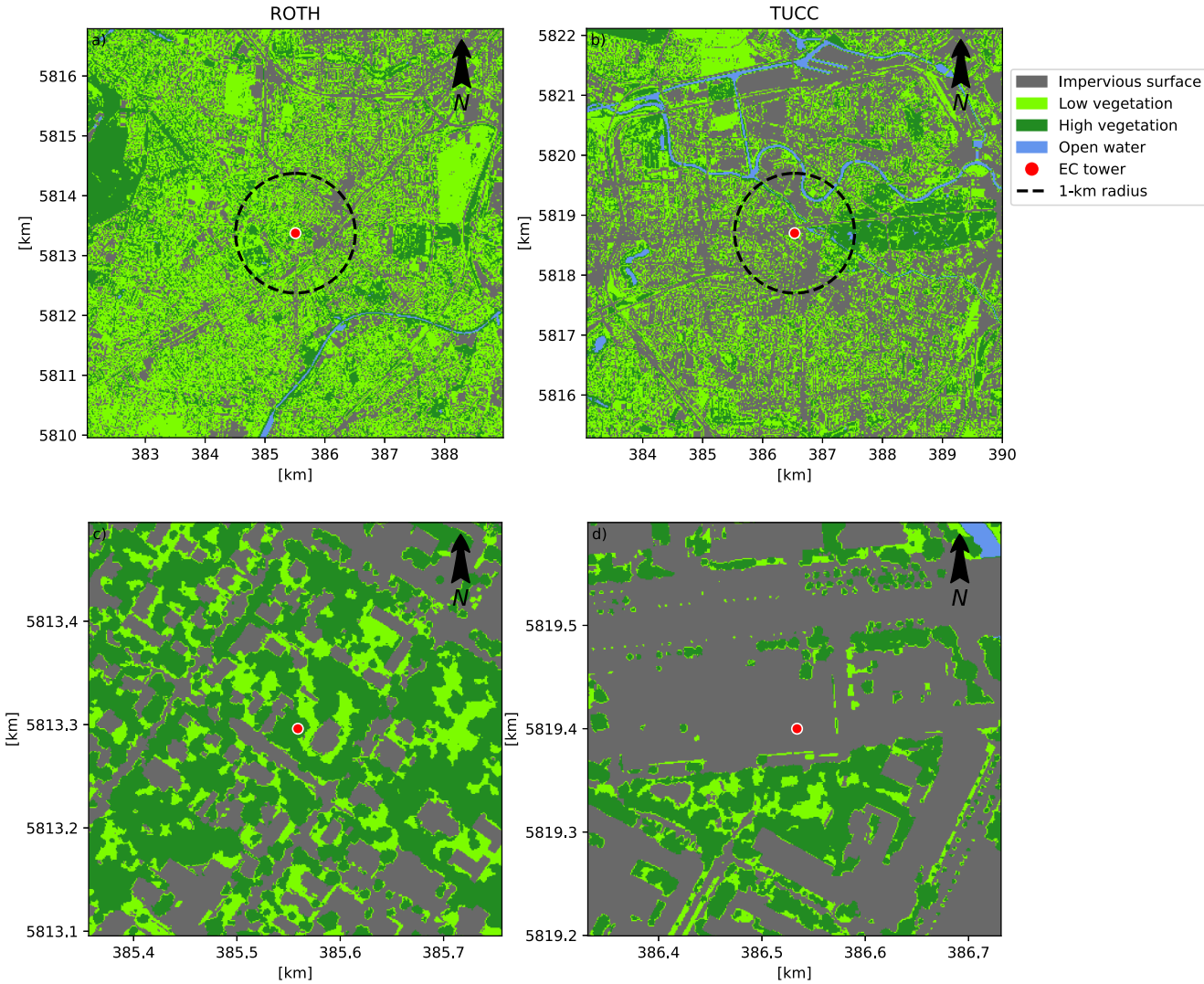

Figure 1. Map of Berlin indicating the location of the (a, c) ROTH and (b, d) TUCC study sites with their surroundings classified in the four surface cover types distinguished in this study with the 1-km radius (dashed black line) around the EC towers (red dots). Panel b and d are zoomed in around the EC towers to show the effect of resampling the 1-m resolution to visualize the full maps (a, b). The coordinate reference system is WGS 84 UTM/33N EPSG: 32633.

Figure 1a (Vulova et al., 2021)). This site is an ICOS (Integrated Carbon Observation System) Associated Ecosystem Station (DE-BeR). The ROTH tower is located in a fairly green and residential neighborhood, with its surroundings within 1 km consisting of 47% impervious surface, 19% low vegetation, 34% high vegetation, and no open water (see Section 3.1). High vegetation is defined as exceeding 0.5 m. The ROTH tower is mainly surrounded by local climate zones 6 (“Open low-rise”), 2 (“Compact midrise”), and 5 (“Open midrise”). Furthermore, the mean building height, vegetation height, and sky view factor (SVF) are 14 m, 7.6 m, and 0.91, respectively, within 1 km of the ROTH tower. The research garden within which the tower is situated consists mainly of grassland (16%), shrub (7%), trees (39%), and semi-permeable or sealed surfaces (16%) (Kuhlemann et al., 2021). The low vegetation is mostly meadow which is mowed 1–2 times per year, with nearly no bare soil in the source area. Most trees at the ROTH site are deciduous and broadleaved, with key species being Acer platanoides, A. pseudoplatanus, A. campestre, Fagus sylvatica, Populus nigra, Platanus acerifolia, Platanus x hybrida, Quercus robur, and Tilia spp. (Gillefalk et al., 2021; Meier & Scherer, 2012). However, evergreen needleleaf conifers are also present in the area (e.g., Taxus baccata, Pinus sylvestris, Abies procera), as well as a deciduous conifer species (Larix decidua). For a more detailed description of the vegetation, we refer to Meier and Scherer (2012); Gillefalk et al. (2021); and Kuhlemann et al. (2021).

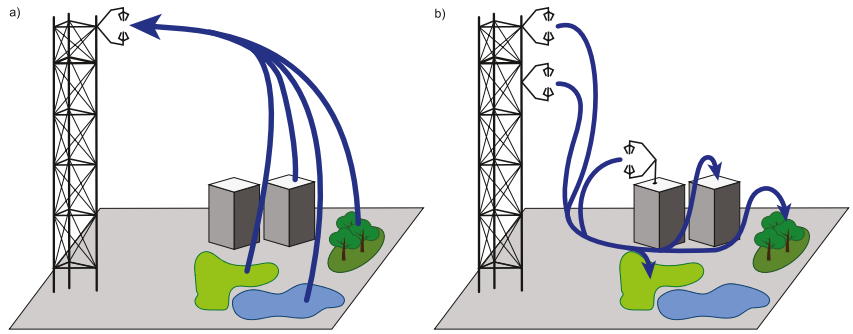

Figure 2. Conceptual drawing of the bottom-up (a) and top-down (b) approach. The arrows start at the data sources and end at the results of the approaches. Footprints determine the contribution for each surface cover type (not shown).

At ROTH, a 40-m tower holds three EC systems (IRGASON, Campbell Scientific) at 2, 30, and 40 m. For all EC systems in this study, the resolution is 30 min. The observations are quality controlled according to the literature and only high-quality data (flag 0) is used (Foken et al., 2004). Additionally, sap flow was observed at six trees with FLGS-TDP XM1000 sap velocity logger systems (Dynamax Inc, Houston, USA), and soil moisture content was measured in two locations below high vegetation at three depths: 10–15, 40–50, and 90–100 cm (CS650 reflectometers, Campbell Scientific) (Kuhlemann et al., 2020). Finally, the leaf area index was measured monthly over three transects through high vegetation (LAI-2200, LI-COR, Lincoln, USA) (Vulova et al., 2019). Along each transect, leaf area index measurements were conducted at 1-m intervals to capture the canopy variability, while walking in the same direction each time for standardization. A tripod on a balcony served as a reference for the above-canopy light conditions measuring every 10 s.

The second site is close to the city center at the TU Berlin Campus Charlottenburg (TUCC, 52.512°N, 13.328°E, Figure 1b (Jin et al., 2021; Vulova et al., 2019)). Its surroundings within 1 km are more impervious than at ROTH: 62% impervious surface, 8% low vegetation, 26% high vegetation, and 3% open water (see Section 3.1). The TUCC site is in a central built-up area mainly occupied by commercial and university buildings beside the nearby Tiergarten Park. It is dominated by local climate zones 2 (“Compact midrise”) and 5 (“Open midrise”). Around the TUCC tower (1-km radius), the mean building height, vegetation height, and SVF are 17.4 m, 9.7 m, and 0.87, respectively. Low vegetation in the TUCC site mainly comprises turfgrasses, with minimal bare soil in the area. Most trees in the TUCC area are also broadleaved and deciduous with the main tree species being Tilia and Acer spp. Irrigation occasionally occurs at both sites (more frequently in ROTH than TUCC) but only during very dry conditions. On the roof of TU Berlin (building height 46 m), observations are made with a ceilometer (Lufft CHM 15 k) and an EC system (IRGASON, Campbell Scientific). The EC system is attached to a 10-m tower reaching 56 m above ground level.

3. Methods

3.1. Surface Cover Classification

The surface cover needs to be classified to link the surface in the EC footprint to the neighborhood-scale *ET* observed with the EC system. Given the surface fraction in the footprint covered by each surface cover type, the *ET* can be reconstructed from the evaporation dynamics of the different surface cover types (bottom-up, Figure 2a) or attributed to the surface cover types by linear decomposition (top-down, Figure 2b). For this study, we classify the surface into four different surface cover types: impervious surface, low vegetation, high vegetation, and open water. For this purpose, we combine information from four geospatial data sets from Berlin Open Data and the Berlin Digital Environmental Atlas.

- *Building height*: raster data set at a 1-m spatial resolution of all buildings in Berlin (Senate Department for Urban Development, Building and Housing, 2012).
- *Vegetation height*: raster data set at a 1-m spatial resolution of all vegetation including trees, bushes, and grass in Berlin (Senate Department for Urban Development, Building and Housing, 2012).

- *Biotope types*: vector data set describing the biotope type of all vegetation in Berlin according to the 7,483 biotope types described by Zimmermann et al. (2015) (Senate Department for Urban Development, Building and Housing, 2013).
- *Streets*: vector data set with all road segments in Berlin (Senate Department for the Environment, Mobility, Consumer and Climate Protection Berlin, 2014).

Around each EC tower, we classified the surface cover within a buffer of 0.025° latitude and 0.05° longitude in both directions, equivalent to 2.8 and 3.4 km. In total, this gives an area of 5.6 by 6.8 km. We selected this buffer, as for 90% of the footprints this area includes the entire footprint calculated in this study (see Section 3.2). For only 0.5% of the time, the buffer contains less than 80% of the footprint. All data sets are clipped to this area. Vector data sets are resampled to rasters at a 1-m resolution to ensure compatibility with the raster data sets.

At the start of the classification, all described vegetated land biotopes are assigned to vegetation and all water biotopes to open water. The impervious surface is determined based on all areas in the street data and all areas that have an assigned building height. The vegetation is split into low and high vegetation depending on the height with a threshold of 0.5 m following Kuhlemann et al. (2021). The exact threshold has minimal influence as only a negligible part of the vegetation has a height between 0.3 and 1.0 m.

3.2. Footprint Modeling

Footprints were calculated to determine the source area of the turbulent fluxes for all timesteps. We selected the flux footprint model from Kljun et al. (2015), which is frequently applied in urban environments (e.g., Karl et al., 2023; Nicolini et al., 2022; Stagakis et al., 2019). This footprint model provides two-dimensional grids outlining the footprints and quantifying the relative weight of each pixel in the footprint. The model requires the measurement height, friction velocity, boundary-layer height, Obukhov length, horizontal wind direction, and mean and standard deviation of the horizontal wind speed. For all wind variables, EC observations are used, while the boundary-layer height is derived from ceilometer observations at the TUCC site. The Obukhov length in m (L) is calculated according to:

$$L = -\frac{u_*^3\,\bar{\theta}_v}{\kappa g\left(\overline{w'\theta_v'}\right)_s} \tag{1}$$

where u_* the surface friction velocity in m s^{-1}, $\bar{\theta}_v$ the mean virtual potential temperature in K, κ the von Kármán constant of 0.4, g the gravitational acceleration of 9.81 m s^{-2}, and $\left(\overline{w'\theta_v'}\right)_s$ the kinematic virtual potential temperature flux in K m s^{-1} at the observation height.

As the model results in contours per 10% and the 100%-contribution contour is infinite, the resulting footprint grids are limited to the 90%-contribution contour. Part of the footprint is not taken into account when the footprint extends beyond the classified area (Section 3.1). This last step had minimal influence, as the classified area is considerably larger than the typically considered representative area within a radius of either 0.5 or 1 km (Lipson et al., 2022). In the end, the contribution of each surface cover type to the footprint is calculated taking into account the relative weight of each pixel resulting from the footprint model.

3.3. Bottom-Up

The bottom-up approach attributes *ET* to the different surface cover types by determining evaporation dynamics for each type (Figure 2a). Therefore, it is hypothesized that EC observations can be accurately reconstructed by considering the ET dynamics of the surface cover types and their respective contributions to the footprint area (see Section 3.4, Equation 5). For the impervious surfaces, open water, and high vegetation interception, evaporation dynamics are estimated based on conceptual models. For the low vegetation and the high vegetation transpiration, observations capture the dynamics. We assume the evaporation dynamics per surface cover type to be similar for ROTH and TUCC, as previous research found their forcing is comparable and can be used interchangeably to predict *ET* with the same accuracy (Duarte Rocha et al., 2022). Negative *ET* observations are omitted, as the conceptual models are not capable of predicting negative fluxes. This filter has a very limited impact on the results, as it excludes only 384 of the 17,780 30-min time intervals. The results are evaluated against EC-observed

$ET_{neigborhood}$ at two timescales, midday and daily, as these consider different aspects of ET. Midday is defined from 11:00 until 15:00 local (10:00–14:00 UTC) time with every half hour considered separately. During these hours, incoming shortwave radiation driving ET is highest. Considering multiple hours minimizes the sampling noise due to the stochastic nature of turbulence even at half-hourly timescales. The daily timescale is relevant for water resources management.

3.3.1. Impervious Surface

Evaporation from impervious surfaces is modeled according to Wouters et al. (2015). Their parameterization includes two processes to mimic the water on an impervious surface: rainfall and evaporation. The impervious surface is characterized by the maximum water storage (w_m) in mm m^{-2} and the maximum wet/evaporative fraction (δ_m). These parameters were determined for Berlin based on 3D-LIDAR scans and found to be 1.03 mm m^{-2} and 13.53% (Haacke, 2022). The evaporative fraction decreases following a power law with an exponent of $-\frac{2}{3}$ depending on the water storage, which follows from the assumption that interception storage capacity linearly depends on the storage depth. Water gain from rainfall is reduced in efficiency when closer to the maximum water storage capacity described by:

$$w(t+\Delta t) = w_m\left(1-\ln\left(1-\left(1-e^{\left(1-\frac{w(t)}{w_m}\right)}\right)e^{-\frac{r_0\Delta t}{w_m}}\right)\right) \tag{2}$$

where, w is the water storage in mm, t time in s, Δt length of the time step in s, and r_0 the rainfall intensity in mm s^{-1}. The formulation assumes constant rainfall during a time step. The evaporation is described by:

$$w(t+\Delta t) = \left(w(t)^{\frac{1}{3}} - \frac{\delta_m E_p \Delta t}{3w_m^{\frac{2}{3}}}\right)^3 \tag{3}$$

where E_p is the potential evaporation. The E_p is calculated according to Penman (1956), further described in Equation 4 and the open water section. Equations 2 and 3 are calculated consecutively for each timestep to get the new water height. The meteorological forcing has a resolution of 30 min, but the conceptual model is run numerically at a 30-s time step to ensure a numerically robust solution with linearly interpolated meteorological forcing.

3.3.2. High Vegetation

The ET from high vegetation consists of transpiration and evaporation of water intercepted by the canopy. The transpiration is derived from observations of the soil moisture content and sap flow as described in Kuhlemann et al. (2021). Soil moisture content observations are used from both the "Trees" and "Shrubs" plots for the transpiration estimation from high vegetation. The soil moisture content reflects the evaporated water volume, but root water uptake does not correlate directly with transpiration apparent from the lag between the two. Therefore, we scale daily soil moisture loss with hourly sap flow observations. This method takes advantage of the correctly timed temporal variation in sap flow observations and the accurate water volume estimate of the soil moisture content observations. Soil moisture loss due to drainage is assumed to be negligible, as the deepest soil moisture observations at 95 cm depth showed no soil moisture loss indicating a drainage flux. Furthermore, soil moisture loss in the lowest layer of observations is not added to the evaporation.

The canopy interception and its evaporation are modeled with the Rutter model that allows for sub-daily resolution (Rutter et al., 1975; Valente et al., 1997). The model partitions rainfall between evaporation from the canopy and trunk, throughfall, and stem flow. Two storages are part of the model: the canopy and the trunk. Both storages evaporate at the potential rate calculated according to the Penman (1956) equation (Equation 4) described in the open water section. Canopy storage capacity depends on the tree species ranging between 0.1 and 3 mm (e.g., Aston, 1979; Baptista et al., 2018; Klaassen et al., 1998; Ramírez et al., 2018), although in exceptional tropical canopies capacities up to 8 mm have been observed (Herwitz, 1985). We assume the canopy storage capacity is linearly related to the leaf area index with a storage of 0.2 mm per unit leaf area (Huang et al., 2017). Leaf area index observations at monthly intervals are interpolated with a univariate spline with four degrees of

freedom. The modeled interception appears to be relatively insensitive to the other parameters set at 0.2 mm for the trunk water storage capacity, 0.015 for the fraction of exceedance of the canopy storage capacity partitioned to stem flow instead of throughfall, and 0.02 for the fraction of evaporation from the stem flow. All of these parameters concern the stem flow, which, on average, accounts for only 2% of the precipitation exceeding the canopy storage capacity (Rutter et al., 1975). The modeled interception evaporation is added to the transpiration to obtain the ET from the high vegetation.

An alternative for both vegetation types would be to model the ET_{patch} with the Penman-Monteith equation (Monteith, 1965). Grimmond and Oke (1991) have adapted this equation to urban environments and included the effect of water limitation. As a preliminary analysis, the adapted Penman-Monteith equation was used to represent vegetation in the bottom-up approach. This analysis showed that the adapted Penman-Monteith equation overestimates ET_{patch}. The estimate is twice as high as the precipitation in the same period.

3.3.3. Low Vegetation

Low vegetation is directly represented by an EC system installed at 2 m directly above the grass at ROTH. In their similar study, Peters et al. (2011) installed an EC system close to the surface of a golf court to estimate the ET from low vegetation. Within a forest, a comparable low EC set-up helped to differentiate the ET components in an environment with more obstacles (Paul-Limoges et al., 2020).

The quality-controlled ET is a direct observation of the low vegetation dynamics when the wind comes from between east (90°) and southwest (230°). Fluxes were considered when suitable for process-focused studies and general analysis (quality flag "0" and "1" according to Foken et al. (2004)).

3.3.4. Open Water

Open water evaporation is estimated with a parameterization of the Penman (1956) equation (De Bruin, 1979):

$$E_p = 37 + 40\overline{u}_{2m}(e_{s,2m} - e_{40m}) \tag{4}$$

where $\overline{u}_{2m}$ is the mean wind speed at 2 m (m s^{-1}), $e_{s,2m}$ the saturated vapor pressure at 2 m (Pa), and e_{40m} the vapor pressure at 40 m (Pa). Equation 4 approximates the evaporation from an infinitely thin water layer ignoring heat storage in the water column. The lack of water temperature observations prevented the use of equations that capture the effect of the heat storage in water on ET (Jansen & Teuling, 2020). Open water is assumed to evaporate at the potential rate. In the case of a negative E_p, evaporation is set to 0.

3.4. Top-Down

The top-down approach takes the neighborhood-scale EC observations and attributes the flux to the different surface cover types by solving a system of equations (Figure 2b). The system consists of three equations related to three EC systems (ROTH: 40 and 30 m; TUCC 56 m). Each equation describes how the ET_{patch} from the surface cover types is combined according to the footprint to yield the EC observation of one system. The evaporation for the three surface cover types results in three unknowns, as the evaporation per surface cover type is assumed similar for all EC systems. Open water is not considered as it covers the least area and only three EC systems are suitable for the analysis. To filter out any timesteps affected by open water, we remove all timesteps with more than 5% open water in the footprint of any of the EC systems. The linear system can be solved, as it has an equal number of equations and unknowns.

$$f_{im,1}E_{im} + f_{lv,1}ET_{lv} + f_{hv,1}ET_{hv} + f_{ow,1}E_{ow} = ET_{EC,1} \tag{5}$$

$$f_{im,2}E_{im} + f_{lv,2}ET_{lv} + f_{hv,2}ET_{hv} + f_{ow,2}E_{ow} = ET_{EC,2} \tag{6}$$

$$f_{im,3}E_{im} + f_{lv,3}ET_{lv} + f_{hv,3}ET_{hv} + f_{ow,3}E_{ow} = ET_{EC,3} \tag{7}$$

where f is the footprint-weighted fraction with the subscripts describing the impervious surface (im), low vegetation (lv), high vegetation (hv), and open water (ow). The numbers indicate the different EC systems. The evaporation from each surface can be determined given the footprint-weighted fractions derived from the

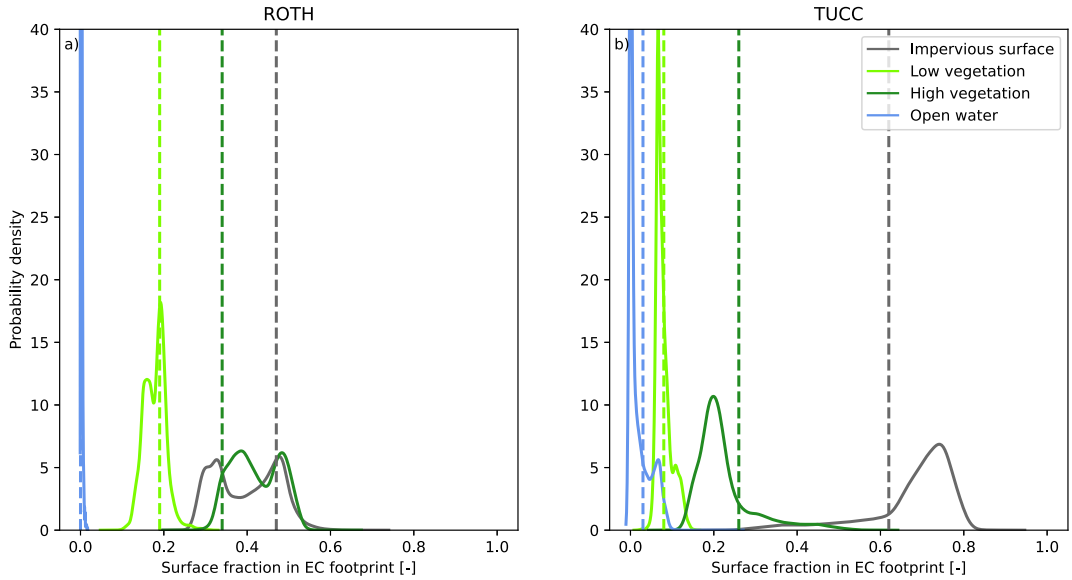

Figure 3. Probability density of the time-dependent footprint-weighted surface fractions in the EC footprint calculated according to Kljun et al. (2015) over the study period (April–October 2019) for ROTH (a) and TUCC (b). The dashed vertical lines indicate the average surface cover fraction within a 1-km radius of the EC (see Figure 1).

footprints and the EC observations. We exclude solutions with estimated evaporation below 0 mm d^{-1} for one of the surface cover types, as these solutions likely have negative evaporation rates for one surface cover type that are balanced by positive evaporation rates for another type.

4. Results

4.1. Footprint Variation

A high variation in footprint composition highlights the heterogeneity of the urban surface (Figure 3). The wide, non-normal distributions cause the footprint-weighted surface fractions in the footprint to differ substantially from the surface cover fractions within a 1-km radius of the EC system (vertical lines) at most times. The 1-km radius estimation and the footprint-weighted fraction are only similar for open water, as this covers a limited surface. For the impervious surface and high vegetation at ROTH, the bi-modality of the distribution demonstrates that a single value will not be able to capture the footprint-weighted surface fractions. Additionally, footprint-weighted surface cover fractions can vary within a wide range as seen at TUCC where the footprint-weighted impervious surface fraction varies from 0.2 up to 0.8. The high variation necessitates that the time-dependent footprint composition is considered to understand *ET* dynamics.

4.2. Surface Cover Composition Impact on Evapotranspiration

Combining the footprint variation from both sites with the EC-observed $ET_{neighborhood}$ reveals the influence of the surface cover composition on *ET* (Figure 4). We find lower *ET* values with more impervious surface and higher *ET* values with more vegetation (high and low). Open water shows a less clear relation between its surface fraction and *ET*, as the range in open water fraction in the footprint is minimal given the limited open water in the proximity of the EC systems (Figure 1). Although the surface cover is relevant, the variation in the *ET* indicates meteorological conditions affect *ET* as well, illustrated by the ordering of the points by available energy quantified as the net radiation. While the surface cover composition in the footprint varies at one site, the two sites together reveal an evident influence of the surface on *ET*.

4.3. Evapotranspiration Attribution to the Surface Cover

EC-observed $ET_{neighborhood}$ is approximated by $ET_{neighborhood}$ reconstructed by a weighted average of surface cover type evaporation dynamics (Figure 5 and Table 1). The negative mean bias error indicates an underestimation of

10.1029/2024WR037508

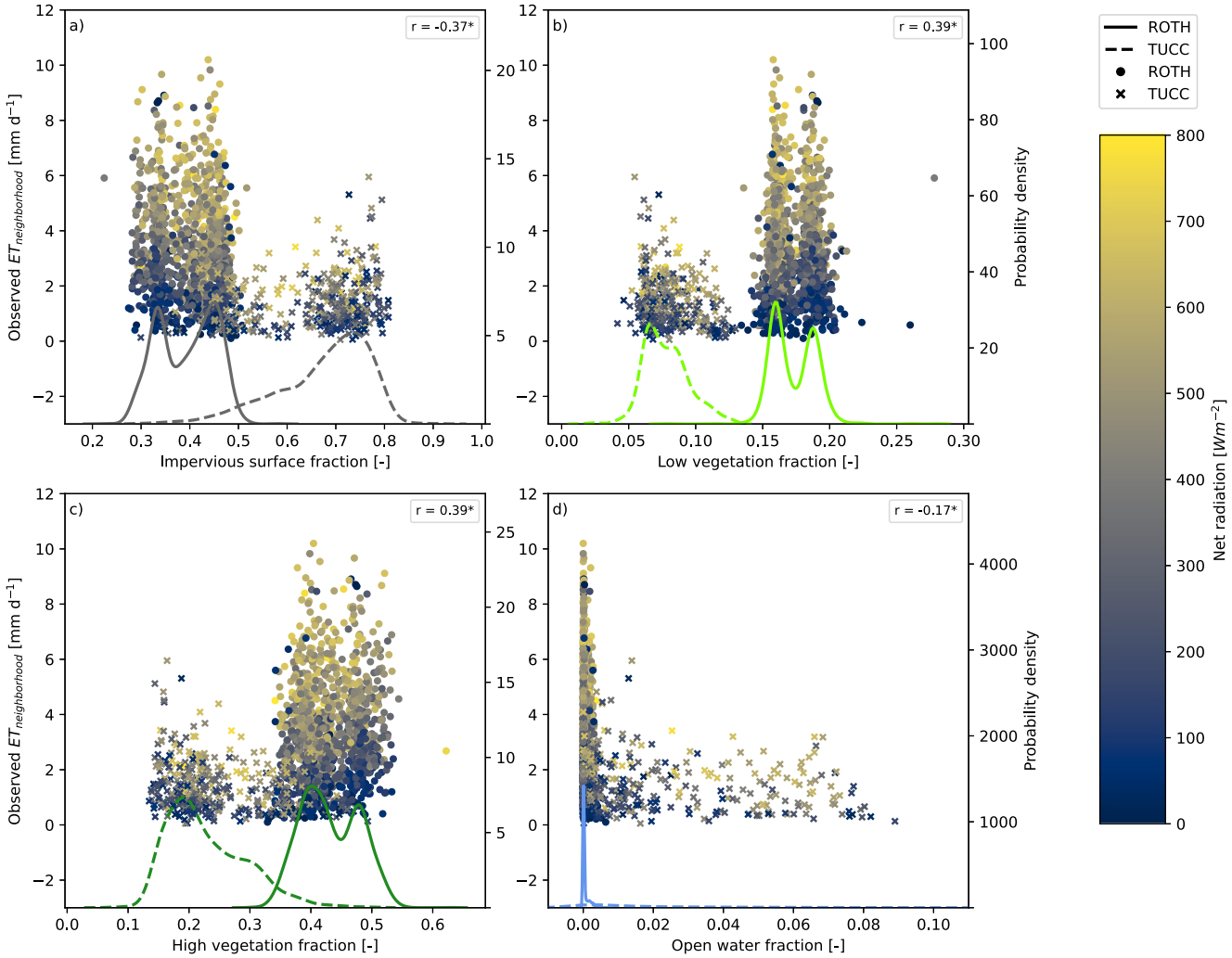

Figure 4. Relation of the EC-observed $ET_{neighborhood}$ and the footprint-weighted surface cover fraction for each surface cover type (a, impervious surface; b, low vegetation; c, high vegetation; d, open water) with the color indicating the net radiation. The probability density curves (right axis) describe the footprint compositions for both ROTH (solid) and TUCC (dashed). The correlation is given in the top right of each panel.

total *ET*. The data gaps due to quality control of the 2-m EC system explain why the number of evaluated data points is lower than the duration of the study period. In one ROTH case, *ET* is highly overestimated when a rainfall event coincides with a high impervious fraction in the footprint and high potential evaporation (Figure 5a), for which the conceptual model for impervious surfaces is responsible.

Impervious surfaces contribute proportionally less to *ET* than their footprint-weighted surface fraction according to the bottom-up approach (Figure 6a). In contrast, high vegetation contributes significantly more. The relative *ET* contribution of low vegetation varies depending on whether the remaining surface fraction in the footprint is dominantly high vegetation or impervious surface, as ET_{patch} from low vegetation is higher than from high vegetation than from impervious surface. Despite open water covering only a small part of the surface, the TUCC results indicate that the $ET_{neighborhood}$ fraction can exceed the footprint-weighted surface fraction. The relative contributions are constant throughout the months, although exact values vary mostly around 0.02 with exceptions up to 0.13. Throughout the study period, the footprint-weighted surface fraction has the same qualitative relation to *ET* contribution.

The top-down approach yields mostly similar relative contributions to the surface cover and *ET* as the bottom-up approach (Figure 6b). However, the $ET_{neighborhood}$ fractions are more similar to the surface fractions than the bottom-up approach indicates. Unfortunately, the open water surfaces could not be considered, as only three EC

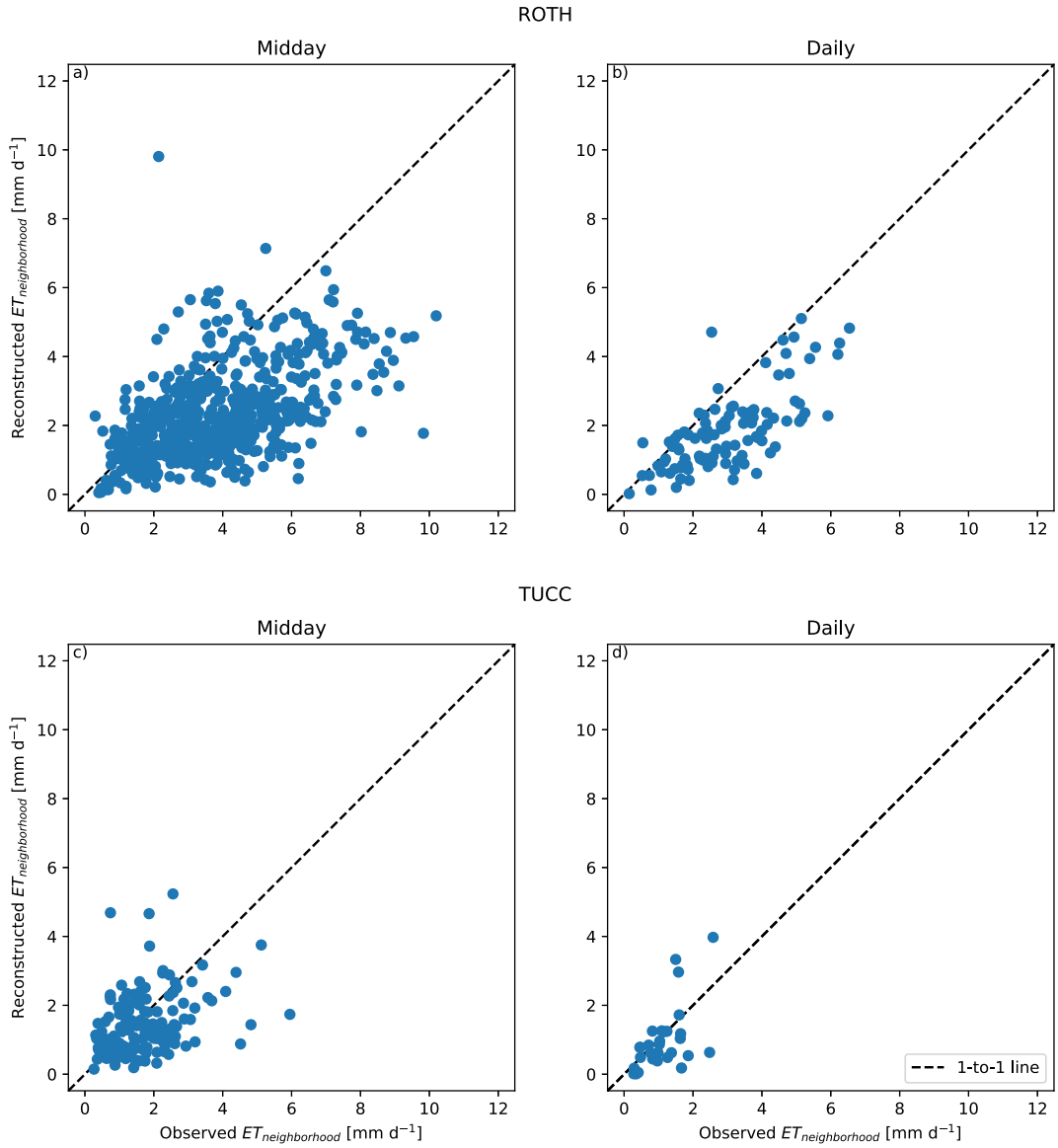

Figure 5. Comparison of the *ET* observed with EC against the *ET* reconstructed with small-scale observations and conceptual models at (a, b) Rothenburgstraße (40 m only) and (c, d) TU Berlin campus for (a, c) midday hours per half hour and (b, d) daily means. Midday hours are between 11:00 and 15:00 local time (10:00–14:00 UTC). Table 1 gives an overview of the statistics.

systems had observations for sufficient timesteps. Still, data gaps cause the top-down approach to yield results for 10,652 timesteps. Subsequently, 9,860 timesteps are excluded from the analysis as negative evaporation rates artificially enhanced the evaporation from the other surfaces. This artificial enhancement is an artifact of the linear system of equations (Equation 5). Next to the $ET_{neighborhood}$ fractions, the footprint-weighted surface fractions differ slightly from the bottom-up approach because different timesteps are considered. Over the months, relative *ET* contributions are less constant than the bottom-up approach typically differing about 0.15 and maximally 0.28. Unlike the bottom-up approach, no direct comparison with observations can be made, as the method gets the EC observations as input, and no observations are available at the patch scale.

4.4. Evaporation Dynamics Per Surface Cover Type

The distinct evaporation dynamics of each surface cover type are visible when zooming in on one drydown (Figure 7). These dynamics can be derived from the bottom-up approach given its good performance and the high

Table 1
Overview of the Performance of the Bottom-Up Approach Compared With EC ET Observations Per 30 Minutes as Shown in Figure 5

		Rothenburgstraße		TU Berlin campus	
		Midday	Daily	Midday	Daily
Figure 5	Panel	a	b	c	d
Data points	(–)	609	100	152	30
Observed mean *ET*	(mm d^{-1})	3.8	3.0	1.7	1.1
Modeled mean *ET*	(mm d^{-1})	2.3	1.9	1.4	1.0
Mean bias error	(mm d^{-1})	−1.5	−1.2	−0.3	−0.1
Mean absolute error	(mm d^{-1})	1.8	1.2	0.8	0.6
Pearson's r	(–)	0.51	0.71	0.38	0.57

number of timesteps with attributed fluxes. The impervious surface has a unique pattern with a sharp peak after rainfall and no evaporation once the surface has dried. Meanwhile, the other three surface cover types all show a daily cycle. Low vegetation and open water show comparable changes over time without a response to the time since the last precipitation but following energy availability and transport efficiency. On the other hand, high vegetation limits *ET* within days after rainfall. These responses are seen in all other dyrdowns except for the last drydowns during the warm season (see Figure A1). At this time, the soil moisture is more depleted triggering low vegetation to limit *ET*, while open water maintains the same response.

5. Discussion and Conclusion

5.1. Surface Cover Type Contributions to Evapotranspiration

Our study revealed that the four distinct surface cover types do not contribute to *ET* proportional to their footprint-weighted surface fraction. To disentangle these contributions, the *ET* was attributed to the surface cover types with both a bottom-up and top-down approach. Both approaches find similar *ET* contributions compared to the footprint-weighted surface fraction; impervious surfaces evaporate less than their footprint-weighted surface fraction, while high vegetation and open water evaporate more. The higher *ET* values for the (high) vegetation are likely explained by the high leaf area (Bian et al., 2019; Y. Liu et al., 2016), which effectively increases the evaporating surface over the same ground surface. The low *ET* values for the impervious surface are likely linked to the low water availability (Jansen et al., 2023; Jongen et al., 2022).

For high vegetation, an isotope-evaluated model study found similar ratios between average surface fraction (~30%) and *ET* contribution (~80%) at ROTH (Gillefalk et al., 2022). From this *ET*, evaporation of interception accounts for 17% of the total precipitation over the study period from April to October. This is comparable to some studies finding values between 14% and 27% (Bryant et al., 2005; Xiao & McPherson, 2011), while others show higher interception evaporation between 45% and 77% (Anys & Weiler, 2023; Asadian & Weiler, 2009) or lower between 5% and 6% (Paul-Limoges et al., 2020). Although our interception evaporation is lower than most observed values, together with transpiration, it exceeds the precipitation during the study period. Soil moisture reserves supply the additional water.

The found *ET* contributions are largely in line with findings by Peters et al. (2011), who did a similar exercise for a more homogeneous neighborhood. Still, we challenge their assumption that the impervious surface did not contribute anything to *ET*, as we find 7% (18% top-down) of *ET* may come from impervious surfaces in a

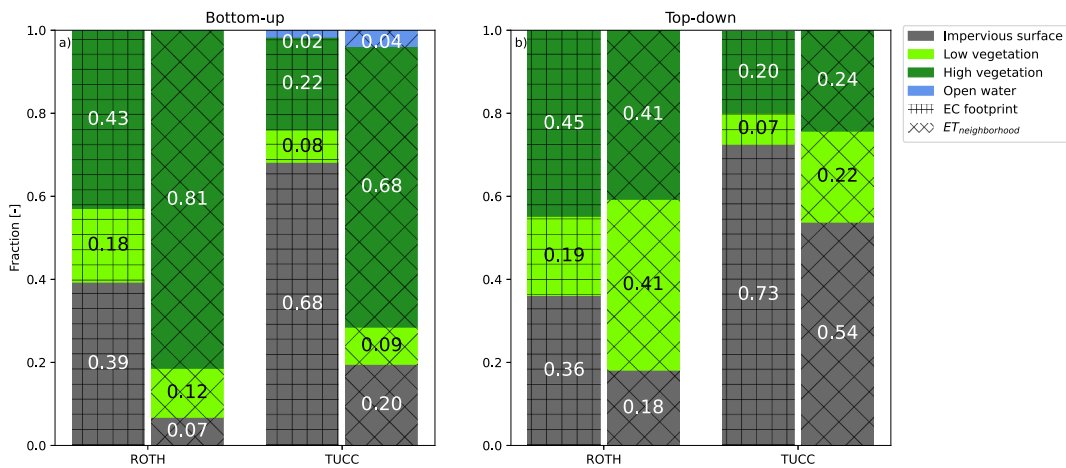

Figure 6. Relative contribution of the surface cover types to the EC footprint (vertical/horizontal hatch) and $ET_{neighborhood}$ (diagonal hatch, calculated as fET_{patch}) for all available 30-min intervals for ROTH (a) and TUCC (b). Surface cover fractions differ between the two methods at the same site at different times and thus footprints are included in the analysis due to data availability.

10.1029/2024WR037508

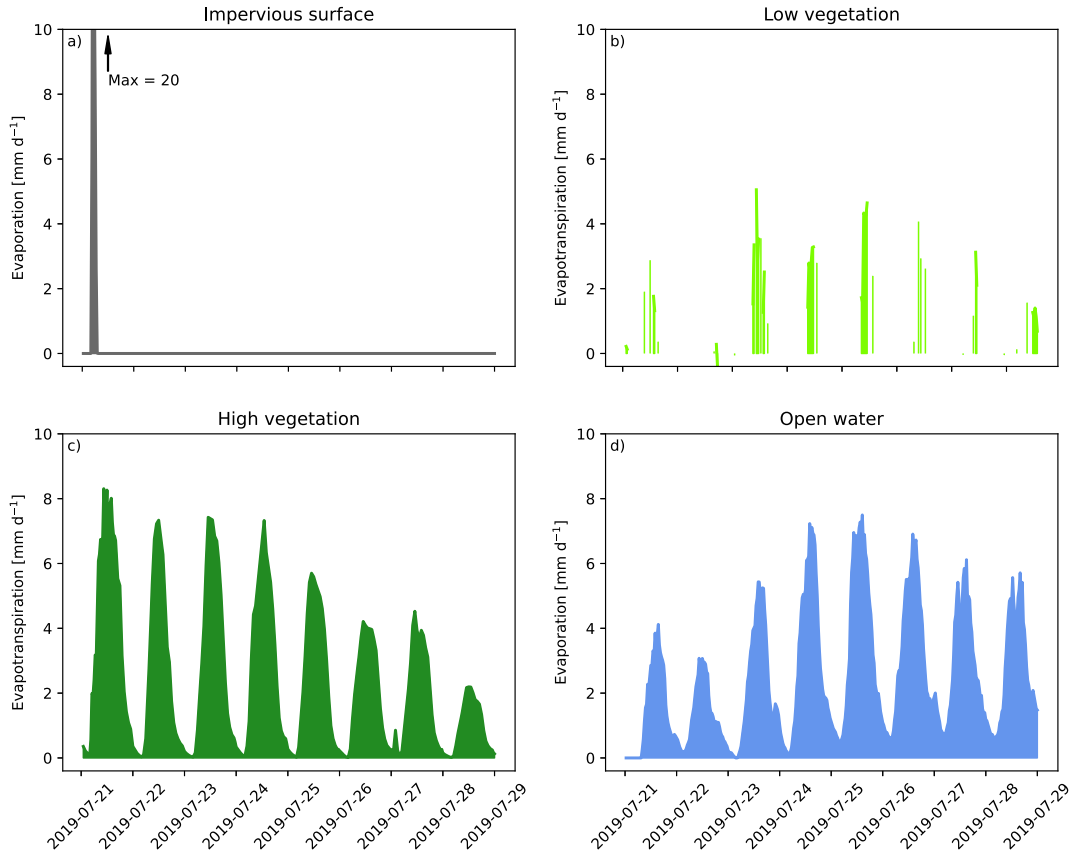

Figure 7. Illustration of *ET* dynamics during a drydown starting 30 min after rainfall ceased determined with the bottom-up approach for the four surface cover types (a, impervious surface; b, low vegetation; c, high vegetation; d, open water). This drydown occurred between 21-07-2019 and 29-07-2019. The gaps in the low vegetation time series are explained by the quality control of the 2-m EC measuring low vegetation.

suburban setting (ROTH, 36/39% impervious in footprint). In the more impervious city center (TUCC, 68/73% impervious in the footprint), we find a contribution of 20% (54% top-down). Ramamurthy and Bou-Zeid (2014) and Chen et al. (2023) found *ET* from impervious surfaces contributed between 11% and 18%.

5.2. Evaporation Dynamics Per Surface Cover Type

Apart from the different *ET* contributions compared to the surface fraction, evaporation evolves differently for each surface cover type after rainfall. In line with Ramamurthy and Bou-Zeid (2014), we find impervious surfaces evaporate all water quickly after rainfall. In contrast, open water sustains evaporation for a longer time. The open water evaporation shows a strong diurnal trend reaching zero during the night, which is incorrect according to the literature. The effect of heat storage could not be considered due to missing water temperature observations. Previous research shows the large heat capacity of water dampens the diurnal trend preventing it from going down to zero (Jansen et al., 2023). In this study, the diurnal trend results from the Penman equation (Jansen & Teuling, 2020), which was applied given the unavailability of water temperatures. High and low vegetation show different behavior from each other with the high vegetation having a higher initial *ET*. While high vegetation decreases peak *ET* within days after the last precipitation, low vegetation sustains high *ET* rates until soil moisture availability is limiting. This soil moisture limitation only occurred toward the end of the summer, even though our study year 2019 was relatively dry. The same responses were found in other studies (Teuling et al., 2010; van Dijke et al., 2023). High vegetation has a stronger stomatal control that enables it to limit transpiration with sufficient available moisture, while low vegetation has lower stomatal control that causes it to limit transpiration less than high vegetation until it lacks water. In the urban setting, low vegetation is also frequently shaded possibly removing the necessity to limit transpiration.

5.3. Bottom-Op Versus Top-Down Approach

Even though the *ET* contribution was similar for the bottom-up and the top-down approach, these methodologies also showed two interesting differences. Given these two differences, we think the bottom-up approach has the most potential to contribute to our understanding of the link between patch- and neighborhood-scale *ET*. The first difference is the need for observations from multiple EC systems simultaneously. Every EC system has gaps in the observations that do not overlap with the other EC systems' gaps. The gaps result from the quality control and are numerous because of the challenging urban environment (Feigenwinter et al., 2012; Oke et al., 2017). The top-down approach requires as many EC systems as surface cover types. In the present study, this was circumvented by excluding open water. Because a fourth EC system was unnecessary, the number of timesteps with a successful outcome rose from 44 to 792. This is comparable with the 751 for bottom-up, for which the availability is mainly limited by the low 2-m EC system with data for only 17% of the time. The maximum number is given by the study period of 244 days equal to 11,712 half hours, of which 2,196 are during the midday hours. While data availability is a challenge for both approaches, the top-down approach relies more heavily on EC observations leading to more overlapping data gaps.

The second difference is that the bottom-up approach is confined by patch-scale observations and models, while the top-down approach is not. The confined bottom-up approach provides insight into the *ET* contributions of the surface cover types but still has a mismatch with the observed *ET*. Also using a bottom-up approach, Salmond et al. (2012) reconstructed the neighborhood-scale sensible heat flux observed with an EC system with smaller-scale observations from two scintillometers. They found a mismatch of 25%, which can partly be explained by three reasons that also apply here. Firstly, even when EC systems are installed directly next to each other, the observations differ, up to 15% in the case of *ET* (Mauder et al., 2006, 2013). These differences are partly due to large turbulent structures that are not resolved at (sub-)hourly timescales. This makes time-averaged EC observations not by definition representative of the spatial average over heterogeneous surfaces. As these structures may resolve at daily timescales, it may explain the better performance of the bottom-up approach at the daily timescale. Secondly, the footprints are calculated with an analytical model that does not account for surface heterogeneity and 3-dimensional surfaces (more in Section 5.4). Lastly, the patch-scale observations are not necessarily representative of the whole neighborhood scale. In our case, for example, sap flow was measured at six trees that cannot capture the diversity of the trees in the EC footprint. Another example is the low vegetation that experiences shading depending on the location within the urban canyon.

Still, the bottom-up approach yields errors comparable to urban land surface models from a decade ago and only slightly higher than more recent models (Grimmond et al., 2011; Lipson et al., 2023). These urban land surface models share our assumption that the neighborhood flux is the sum of ET_{patch} from the separate surface cover types. They do not incorporate dynamic footprint information in the forcing but use the direct surroundings or an average footprint (Lipson et al., 2023). As our approach reduces complexity and requires fewer inputs, we demonstrate the relevance of these footprints in scaling patch fluxes to the neighborhood level. The added complexity of urban land surface models allows for prediction and scenario studies, which our approach would not be suitable for. Still, the found agreement underscores the potential for utilizing surface-specific contributions to decipher *ET* dynamics.

In contrast, the top-down approach yields highly unlikely results as the linear system follows is not confined by patch-scale observations. The linear system counteracted high negative fluxes with high positive fluxes giving results as extreme as -2.0×10^{17} and 1.1×10^{6} mm d^{-1}. These effects were omitted from the analysis by excluding negative fluxes, which omitted the high fluxes as well due to the linear relations in the equations. Due to these direct links, the *ET* contributions contain the errors from the EC observations. However, these random errors will cancel out against each other, as we only look at aggregated results from the top-down results.

5.4. Footprint Variability and Modeling

Given these differences in evaporation behavior between surface cover types, the surface composition in the footprint influences the EC observations. This changing footprint has to be accounted for to understand *ET* dynamics, as the footprint contribution of a particular surface cover type may vary as much as 50%. Previously, the relevance of footprints for *ET* was illustrated by the improved performance when the footprint-weighed surface cover fraction was supplied to machine learning models in addition to meteorological observations

(Vulova et al., 2021, 2023). This is the first process-based study that reveals how *ET* dynamics differ from hour to hour per surface cover type. For other fluxes, such as CO_2, footprint modeling has also been shown to help understand flux dynamics (e.g., Conte & Contini, 2019; Velasco et al., 2009; Wu et al., 2022).

CO_2 sources including directly from humans have been identified and quantified by looking at the relation between the CO_2 flux and the surface cover composition equivalent to Figure 4. One example is Menzer and McFadden (2017) who study the relative importance of vegetation and anthropogenic fluxes of CO_2. Another example is Stagakis et al. (2019) who find that traffic is an important CO_2 source and human respiration accounts for 19% of the CO_2 flux. Human respiration and perspiration are unlikely to affect our results. In the center of Beijing, the water fluxes from these processes are so small they would account for only 3% of *ET* in Berlin (C. Liu et al., 2022). Given the lower population density of our sites, human respiration and perspiration are even lower. Thus, these small water fluxes from these sources are much smaller than *ET* and do not influence the results.

Footprint modeling is the key that connects the surface to the *ET* in this study. The key is however limited by the simplifications of the footprint model. Here, we applied the analytical model by Kljun et al. (2015), which generates perfectly symmetrical footprints. The model does not account for the complexity and heterogeneity of the urban morphology. More detailed footprint modeling would provide footprints depending on urban morphology, but this would also require more computational resources and thus limit the length of the period that can be studied.

5.5. Generalizability

Here, we studied *ET* in one city during the warm months of a single year, 2019, which was a relatively dry year in Berlin. While the climate and year-to-year variability may affect some aspects of the *ET* dynamics, others are likely to be more constant. The main aspect we expect to be relatively constant is the evolution of *ET* over a drydown. The impervious surface will evaporate with a short intense peak, open water will evaporate more constantly, and vegetation will respond to soil moisture. While open water contributes little to the surface cover, we included this surface cover type in our analysis. It cannot be assigned to any of the other surface cover types and its inclusion improves the transferability of our methodology. The general patterns may be the same, but the dynamics are altered by site characteristics such as plant species, building materials, and water depth. The urban morphology is another relevant site characteristic that affects the incoming energy by providing more or less shading related to the height-width ratio. Still, we anticipate these effects to be smaller than the differences between the four surface cover types. Apart from site characteristics, weather conditions control how much each of the surface cover types contributes to the *ET* (Jansen et al., 2023). The weather conditions determine the water availability (number and length of drydowns), energy availability (radiation and temperature), and exchange efficiency (wind and vapor pressure deficit). These conditions will lead to changed *ET* dynamics dependent on the season, the climate, and the year-to-year variability.

The unique 2019 data set from Berlin allowed us to reconstruct the *ET* signal from EC systems. Although relatively common observations are required for the conceptual models of the open water and impervious surfaces, the data needed to estimate the evaporation dynamics of both vegetated surfaces is more specialized. These observations included low-level EC observations, tree sap flow, and multiple, continuous soil moisture sensors. In most cities, this will not be available. Instead, the vegetated surfaces could be modeled with the Penman-Monteith equation (Monteith, 1965). However, our preliminary analysis showed a severe overestimation of *ET* from vegetation. Without further adaptation, $ET_{neighborhood}$ cannot be reconstructed with the Penman-Monteith equation using less specialized observations.

6. Conclusion

This study explores the link of neighborhood-scale *ET* to the surface cover at two sites in Berlin to estimate the contribution of each surface cover type to *ET*. This link is made starting from the *ET* dynamic from the surface cover types reconstructing the neighborhood-scale flux (bottom-up) and from four neighborhood-scale fluxes partitioned over the surface cover types through a linear system of equations (top-down). The bottom-up approach demonstrates that patch-scale dynamics can reconstruct the neighborhood scale when the EC footprint is considered.

Impervious surfaces contribute substantially to *ET* after rainfall mounting up on long timescales and are thus not negligible as assumed in earlier studies. That is why they should also not be ignored in urban water management. In line with previous studies, we find most *ET* originates from vegetation with especially high vegetation evaporating disproportionately more than its footprint-weighted surface fraction. While both approaches support these conclusions, the bottom-up approach proved to be more successful than the top-down approach in linking the surface cover types at the patch scale to the observations at the neighborhood scale due to its lower EC data requirement.

We stress the importance of time-dependent EC footprints to understand *ET* dynamics. Based on these dynamics, urban land surface models and their evaluation could be improved by accounting for the changing footprint. With footprint information, parameters could be dependent on the situation in the current source area. In this way, the models would more directly represent what the EC system observes making for a more fair and better evaluation.

Understanding *ET* is crucial in urban water management, for example, to determine appropriate vegetation species and irrigation requirements. At the same time, *ET* plays a role in the energy balance and can contribute to the mitigation of heat stress. Therefore, the gained insights can support design decisions in city landscapes and urban water management to improve the living environment of urban inhabitants.

Appendix A: Drydown at the End of the Warm Season

See Figure A1.

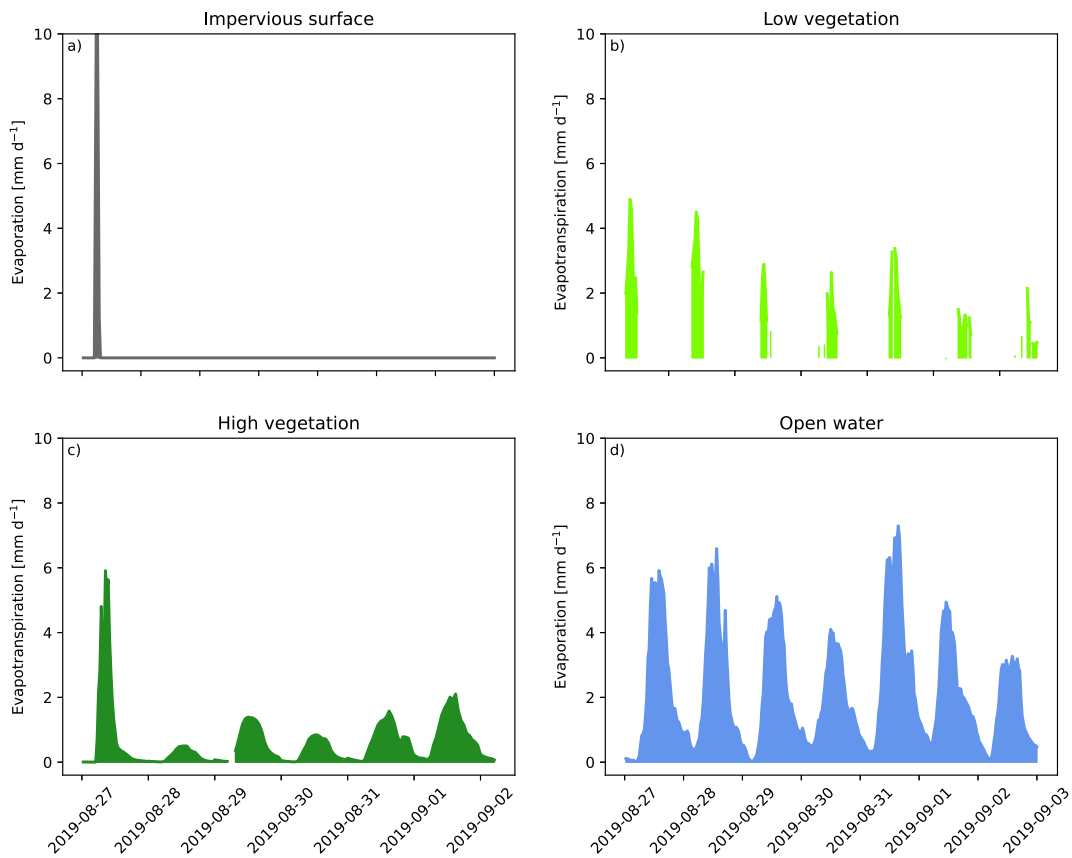

Figure A1. As Figure 7, but for one of the last drydowns of the warm season (a, impervious surface; b, low vegetation; c, high vegetation; d, open water). This drydown occurred between 27-08-2019 and 03-09-2019.

Data Availability Statement

Spatial data sets are available at the Berlin Digital Environmental Atlas (Senate Department for the Environment, Mobility, Consumer and Climate Protection Berlin, 2014; Senate Department for Urban Development, Building and Housing, 2012; Senate Department for Urban Development, Building and Housing, 2013). Rainfall observations can be accessed at the DWD Climate Data Center (DWD, 2021a). Sap flow and soil moisture data are available at the FRED open-access database of IGB (Kuhlemann et al., 2020). All other data in this publication is available at 4TU (Jongen et al., 2024).

Acknowledgments
Special thanks to Judith Boekee, Studio Scientist, for the design of the conceptual figure, her tireless support, and her eye for detail. Harro Jongen acknowledges this research was supported by the WIMEK PhD Grant 2020. Stenka Vulova was supported by the German Research Foundation (DFG) within the Research Training Group "Urban Water Interfaces" (GRK 2032-2). Fred Meier acknowledges funding for instrumentation of the Urban Climate Observatory (UCO) Berlin from DFG Grants SCHE 750/8 and SCHE 750/9 within Research Unit 1736 "Urban Climate and Heat Stress in Mid Latitude Cities in View of Climate Change (UCaHS)" and the research program "Urban Climate Under Change ([UC]2)", funded by the German Ministry of Research and Education (FKZ 01LP1602A).

References

Amt für Statistik Berlin-Brandenburg. (2019). Das statistische informationssystem Berlin-Brandenburg. Retrieved from https://statis.statistik-berlin-brandenburg.de/webapi/jsf/tableView/tableView.xhtml

Anys, M., & Weiler, M. (2023). Rainfall interception of urban trees: Event characteristics and tree morphological traits. *Preprint*, *38*(4), e15146.

Asadian, Y., & Weiler, M. (2009). A new approach in measuring rainfall interception by urban trees in coastal British Columbia. *Water Quality Research Journal*, *44*(1), 16–25. https://doi.org/10.2166/wqrj.2009.003

Aston, A. (1979). Rainfall interception by eight small trees. *Journal of Hydrology*, *42*(3–4), 383–396. https://doi.org/10.1016/0022-1694(79)90057-x

Auvinen, M., Järvi, L., Hellsten, A., Rannik, Ü., & Vesala, T. (2017). Numerical framework for the computation of urban flux footprints employing large-eddy simulation and Lagrangian stochastic modeling. *Geoscientific Model Development*, *10*(11), 4187–4205. https://doi.org/10.5194/gmd-10-4187-2017

Baptista, M. D., Livesley, S. J., Parmehr, E. G., Neave, M., & Amati, M. (2018). Variation in leaf area density drives the rainfall storage capacity of individual urban tree species. *Hydrological Processes*, *32*(25), 3729–3740. https://doi.org/10.1002/hyp.13255

Bian, Z., Gu, Y., Zhao, J., Pan, Y., Li, Y., Zeng, C., & Wang, L. (2019). Simulation of evapotranspiration based on leaf area index, precipitation and pan evaporation: A case study of Poyang lake watershed, China. *Ecohydrology and Hydrobiology*, *19*(1), 83–92. https://doi.org/10.1016/j.ecohyd.2018.03.005

Boese, S., Jung, M., Carvalhais, N., Teuling, A. J., & Reichstein, M. (2019). Carbon–water flux coupling under progressive drought. *Biogeosciences*, *16*(13), 2557–2572. https://doi.org/10.5194/bg-16-2557-2019

Bonneau, J., Fletcher, T. D., Costelloe, J. F., Poelsma, P. J., James, R. B., & Burns, M. J. (2018). Where does infiltrated stormwater go? Interactions with vegetation and subsurface anthropogenic features. *Journal of Hydrology*, *567*, 121–132. https://doi.org/10.1016/j.jhydrol.2018.10.006

Bryant, M. L., Bhat, S., & Jacobs, J. M. (2005). Measurements and modeling of throughfall variability for five forest communities in the Southeastern US. *Journal of Hydrology*, *312*(1–4), 95–108. https://doi.org/10.1016/j.jhydrol.2005.02.012

Chen, H., Huang, J. J., Liang, H., Wang, W., Li, H., Wei, Y., et al. (2023). Can evaporation from urban impervious surfaces be ignored? *Journal of Hydrology*, *616*, 128582. https://doi.org/10.1016/j.jhydrol.2022.128582

Conte, M., & Contini, D. (2019). Size-resolved particle emission factors of vehicular traffic derived from urban eddy covariance measurements. *Environmental Pollution*, *251*, 830–838. https://doi.org/10.1016/j.envpol.2019.05.029

De Bruin, H. (1979). Neerslag, openwaterverdamping en potentieel neerslagoverschot in Nederland, frequentieverdelingen in het groeiseizoen. WR, 79–04.

Duarte Rocha, A., Vulova, S., van der Tol, C., Förster, M., & Kleinschmit, B. (2022). Modelling hourly evapotranspiration in urban environments with scope using open remote sensing and meteorological data. *Hydrology and Earth System Sciences*, *26*(4), 1111–1129. https://doi.org/10.5194/hess-26-1111-2022

DWD. (2021a). DWD Climate Data Center (CDC) [Dataset]. Retrieved from https://opendata.dwd.de/climate_environment/CDC/observations_germany/climate/

DWD. (2021b). Vieljährige mittelwerte [Dataset]. Retrieved from https://www.dwd.de/DE/leistungen/klimadatendeutschland/vielj_mittelwerte.html

Feigenwinter, C., Vogt, R., & Christen, A. (2012). Eddy covariance measurements over urban areas. *Eddy covariance: A practical guide to measurement and data analysis*, 377–397. https://doi.org/10.1007/978-94-007-2351-1_16

Fenner, D., Christen, A., Chrysoulakis, N., Grimmond, S., Van Hove, M., Kotthaus, S., et al. (2023). Impact of a large isolated city on the mixed layer height during different weather conditions (Tech. Rep.). *Copernicus Meetings*.

Fenner, D., Meier, F., Scherer, D., & Polze, A. (2014). Spatial and temporal air temperature variability in Berlin, Germany, during the years 2001–2010. *Urban Climate*, *10*, 308–331. https://doi.org/10.1016/j.uclim.2014.02.004

Fletcher, T. D., Andrieu, H., & Hamel, P. (2013). Understanding, management and modelling of urban hydrology and its consequences for receiving waters: A state of the art. *Advances in Water Resources*, *51*, 261–279. https://doi.org/10.1016/j.advwatres.2012.09.001

Foken, T., Göockede, M., Mauder, M., Mahrt, L., Amiro, B., & Munger, W. (2004). Post-field data quality control. In *Handbook of micrometeorology: A guide for surface flux measurement and analysis* (pp. 181–208). Springer.

Gillefalk, M., Tetzlaff, D., Hinkelmann, R., Kuhlemann, L.-M., Smith, A., Meier, F., et al. (2021). Quantifying the effects of urban green space on water partitioning and ages using an isotope-based ecohydrological model. *Hydrology and Earth System Sciences*, *25*(6), 3635–3652. https://doi.org/10.5194/hess-25-3635-2021

Gillefalk, M., Tetzlaff, D., Marx, C., Smith, A., Meier, F., Hinkelmann, R., & Soulsby, C. (2022). Estimates of water partitioning in complex urban landscapes with isotope-aided ecohydrological modelling. *Hydrological Processes*, *36*(3), e14532. https://doi.org/10.1002/hyp.14532

Grimmond, C. S. B., Blackett, M., Best, M. J., Baik, J.-J., Belcher, S., Beringer, J., et al. (2011). Initial results from phase 2 of the international urban energy balance model comparison. *International Journal of Climatology*, *31*(2), 244–272. https://doi.org/10.1002/joc.2227

Grimmond, C. S. B., & Oke, T. R. (1991). An evapotranspiration-interception model for urban areas. *Water Resources Research*, *27*(7), 1739–1755. https://doi.org/10.1029/91wr00557

Gunawardena, K. R., Wells, M. J., & Kershaw, T. (2017). Utilising green and bluespace to mitigate urban heat island intensity. *Science of the Total Environment*, *584*, 1040–1055. https://doi.org/10.1016/j.scitotenv.2017.01.158

Haacke, N. (2022). Scaling and connectivity assessment of critical source areas of diffuse pollution in urban catchments under a changing regime of high-intensity storms. [PhD thesis]. *Technische Universität Berlin*. https://doi.org/10.14279/depositonce-16434

Heaviside, C., Macintyre, H., & Vardoulakis, S. (2017). The urban heat island: Implications for health in a changing environment. *Current environmental health reports*, *4*(3), 296–305. https://doi.org/10.1007/s40572-017-0150-3

Hellsten, A., Luukkonen, S.-M., Steinfeld, G., Kanani-Sühring, F., Markkanen, T., Järvi, L., et al. (2015). Footprint evaluation for flux and concentration measurements for an urban-like canopy with coupled Lagrangian stochastic and large-eddy simulation models. *Boundary-Layer Meteorology*, *157*(2), 191–217. https://doi.org/10.1007/s10546-015-0062-4

Herwitz, S. R. (1985). Interception storage capacities of tropical rainforest canopy trees. *Journal of Hydrology*, *77*(1–4), 237–252. https://doi.org/10.1016/0022-1694(85)90209-4

Hsieh, C.-I., Siqueira, M., Katul, G., & Chu, C.-R. (2003). Predicting scalar source-sink and flux distributions within a forest canopy using a 2-D Lagrangian stochastic dispersion model. *Boundary-Layer Meteorology*, *109*(2), 113–138. https://doi.org/10.1023/a:1025461906331

Huang, J. Y., Black, T., Jassal, R., & Lavkulich, L. L. (2017). Modelling rainfall interception by urban trees. *Canadian Water Resources Journal/Revue Canadienne des Ressources Hydriques*, *42*(4), 336–348. https://doi.org/10.1080/07011784.2017.1375865

Jacobs, C., Klok, L., Bruse, M., Cortesão, J., Lenzholzer, S., & Kluck, J. (2020). Are urban water bodies really cooling? *Urban Climate*, *32*, 100607. https://doi.org/10.1016/j.uclim.2020.100607

Jansen, F. A., Jongen, H. J., Jacobs, C. M., Bosveld, F. C., Buzacott, A. J., Heusinkveld, B. G., et al. (2023). Land cover control on the drivers of evaporation and sensible heat fluxes: An observation-based synthesis for The Netherlands. *Water Resources Research*, *59*(11), e2022WR034361. https://doi.org/10.1029/2022wr034361

Jansen, F. A., & Teuling, A. J. (2020). Evaporation from a large lowland reservoir–(dis) agreement between evaporation models from hourly to decadal timescales. *Hydrology and Earth System Sciences*, *24*(3), 1055–1072. https://doi.org/10.5194/hess-24-1055-2020

Jansen, F. A., Uijlenhoet, R., Jacobs, C. M., & Teuling, A. J. (2022). Evaporation from a large lowland reservoir–observed dynamics and drivers during a warm summer. *Hydrology and Earth System Sciences*, *26*(11), 2875–2898. https://doi.org/10.5194/hess-26-2875-2022

Jin, L., Schubert, S., Fenner, D., Meier, F., & Schneider, C. (2021). Integration of a building energy model in an urban climate model and its application. *Boundary-Layer Meteorology*, *178*(2), 249–281. https://doi.org/10.1007/s10546-020-00569-y

Jongen, H. J., Steeneveld, G.-J., Beringer, J., Christen, A., Chrysoulakis, N., Fortuniak, K., et al. (2022). Urban water storage capacity inferred from observed evapotranspiration recession. *Geophysical Research Letters*, *49*(3), e2021GL096069. https://doi.org/10.1029/2021gl096069

Jongen, H. J., Vulova, S., Meier, F., Steeneveld, G.-J., Jansen, F. A., Tetzlaff, D., et al. (2024). Data underlying the article "Attributing urban evapotranspiration from eddy-covariance to surface cover: Bottom-up versus top-down [Dataset]. *4TU.ResearchData*. https://doi.org/10.4121/bf56f3d1-d522-44d3-8371-9f2af7a01378

Karl, T., Lamprecht, C., Graus, M., Cede, A., Tiefengraber, M., Vila-Guerau de Arellano, J., et al. (2023). High urban NO_x triggers a substantial chemical downward flux of ozone. *Science Advances*, *9*(3), eadd2365. https://doi.org/10.1126/sciadv.add2365

Klaassen, W., Bosveld, F., & De Water, E. (1998). Water storage and evaporation as constituents of rainfall interception. *Journal of Hydrology*, *212*, 36–50. https://doi.org/10.1016/s0022-1694(98)00200-5

Kljun, N., Calanca, P., Rotach, M., & Schmid, H. P. (2015). A simple two-dimensional parameterisation for Flux Footprint Prediction (FFP). *Geoscientific Model Development*, *8*(11), 3695–3713. https://doi.org/10.5194/gmd-8-3695-2015

Kljun, N., Rotach, M., & Schmid, H. (2002). A three-dimensional backward Lagrangian footprint model for a wide range of boundary-layer stratifications. *Boundary-Layer Meteorology*, *103*(2), 205–226. https://doi.org/10.1023/a:1014556300021

Kormann, R., & Meixner, F. X. (2001). An analytical footprint model for non-neutral stratification. *Boundary-Layer Meteorology*, *99*(2), 207–224. https://doi.org/10.1023/a:1018991015119

Kottek, M., Grieser, J., Beck, C., Rudolf, B., & Rubel, F. (2006). World map of the Köppen-Geiger climate classification updated.

Kuhlemann, L.-M., Tetzlaff, D., Smith, A., Kleinschmit, B., & Soulsby, C. (2020). Soil moisture data for grassland, shrub and trees at the Steglitz urban ecohydrological observatory [Dataset]. *IGB Leibniz-Institute of Freshwater Ecology and Inland Fisheries*. https://doi.org/10.18728/566.0

Kuhlemann, L.-M., Tetzlaff, D., Smith, A., Kleinschmit, B., & Soulsby, C. (2021). Using soil water isotopes to infer the influence of contrasting urban green space on ecohydrological partitioning. *Hydrology and Earth System Sciences*, *25*(2), 927–943. https://doi.org/10.5194/hess-25-927-2021

Leclerc, M. Y., Shen, S., & Lamb, B. (1997). Observations and large-eddy simulation modeling of footprints in the lower convective boundary layer. *Journal of Geophysical Research*, *102*(D8), 9323–9334. https://doi.org/10.1029/96jd03984

Lipson, M. J., Grimmond, C. S. B., Best, M., Abramowitz, G., Coutts, A., Tapper, N., et al. (2023). Evaluation of 30 urban land surface models in the urban-plumber project: Phase 1 results. *Quarterly journal of the Royal Meteorological Society*, *150*(758), 126–169. https://doi.org/10.1002/qj.4589

Lipson, M. J., Grimmond, S., Best, M., Chow, W. T., Christen, A., Chrysoulakis, N., et al. (2022). Harmonized gap-filled datasets from 20 urban flux tower sites. *Earth System Science Data*, *14*(11), 5157–5178. https://doi.org/10.5194/essd-14-5157-2022

Liu, C., Liu, J., Shao, W., Lu, J., & Gao, H. (2022). The considerable water evaporation induced by human perspiration and respiration in megacities: Quantifying method and case study in Beijing. *International Journal of Environmental Research and Public Health*, *19*(14), 8638. https://doi.org/10.3390/ijerph19148638

Liu, Y., Xiao, J., Ju, W., Xu, K., Zhou, Y., & Zhao, Y. (2016). Recent trends in vegetation greenness in China significantly altered annual evapotranspiration and water yield. *Environmental Research Letters*, *11*(9), 094010. https://doi.org/10.1088/1748-9326/11/9/094010

Mauder, M., Cuntz, M., Drüe, C., Graf, A., Rebmann, C., Schmid, H. P., et al. (2013). A strategy for quality and uncertainty assessment of long-term eddy-covariance measurements. *Agricultural and Forest Meteorology*, *169*, 122–135. https://doi.org/10.1016/j.agrformet.2012.09.006

Mauder, M., Liebethal, C., Göckede, M., Leps, J.-P., Beyrich, F., & Foken, T. (2006). Processing and quality control of flux data during litfass-2003. *Boundary-Layer Meteorology*, *121*(1), 67–88. https://doi.org/10.1007/s10546-006-9094-0

McGrane, S. J. (2016). Impacts of urbanisation on hydrological and water quality dynamics, and urban water management: A review. *Hydrological Sciences Journal*, *61*(13), 2295–2311. https://doi.org/10.1080/02626667.2015.1128084

Meier, F., & Scherer, D. (2012). Spatial and temporal variability of urban tree canopy temperature during summer 2010 in Berlin, Germany. *Theoretical and Applied Climatology*, *110*(3), 373–384. https://doi.org/10.1007/s00704-012-0631-0

Menzer, O., & McFadden, J. P. (2017). Statistical partitioning of a three-year time series of direct urban net CO_2 flux measurements into biogenic and anthropogenic components. *Atmospheric Environment*, *170*, 319–333. https://doi.org/10.1016/j.atmosenv.2017.09.049

Monteith, J. L. (1965). Evaporation and environment. In *Symposia of the society for experimental biology* (Vol. 19, pp. 205–234).

Nicolini, G., Antoniella, G., Carotenuto, F., Christen, A., Ciais, P., Feigenwinter, C., et al. (2022). Direct observations of CO_2 emission reductions due to Covid-19 lockdown across European urban districts. *Science of the Total Environment*, *830*, 154662. https://doi.org/10.1016/j.scitotenv.2022.154662

Oke, T. R. (1982). The energetic basis of the urban heat island. *The Quarterly Journal of the Royal Meteorological Society*, *108*(455), 1–24. https://doi.org/10.1002/qj.49710845502

Oke, T. R., Mills, G., Christen, A., & Voogt, J. A. (2017). *Urban climates*. Cambridge University Press.
Paul, M., & Meyer, J. (2001). Streams in the urban landscape. *Annual Review of Ecology and Systematics*, *32*(1), 333–365. https://doi.org/10.1146/annurev.ecolsys.32.081501.114040
Paul-Limoges, E., Wolf, S., Schneider, F. D., Longo, M., Moorcroft, P., Gharun, M., & Damm, A. (2020). Partitioning evapotranspiration with concurrent eddy covariance measurements in a mixed forest. *Agricultural and Forest Meteorology*, *280*, 107786. https://doi.org/10.1016/j.agrformet.2019.107786
Penman, H. (1956). Evaporation: An introductory survey. *Netherlands Journal of Agricultural Science*, *4*(1), 9–29. https://doi.org/10.18174/njas.v4i1.17768
Peters, E. B., Hiller, R. V., & McFadden, J. P. (2011). Seasonal contributions of vegetation types to suburban evapotranspiration. *Journal of Geophysical Research*, *116*(G1), G01003. https://doi.org/10.1029/2010jg001463
Qin, L., Yan, C., Yu, L., Chai, M., Wang, B., Hayat, M., et al. (2022). High-resolution Spatio-temporal characteristics of urban evapotranspiration measured by unmanned aerial vehicle and infrared remote sensing. *Building and Environment*, *222*, 109389. https://doi.org/10.1016/j.buildenv.2022.109389
Ramamurthy, P., & Bou-Zeid, E. (2014). Contribution of impervious surfaces to urban evaporation. *Water Resources Research*, *50*(4), 2889–2902. https://doi.org/10.1002/2013wr013909
Ramírez, B. H., Melsen, L. A., Ganzeveld, L., Leemans, R., & Teuling, A. J. (2018). Tropical montane cloud forests in the Orinoco river basin: Inferring fog interception from through-fall dynamics. *Agricultural and Forest Meteorology*, *260*, 17–30. https://doi.org/10.1016/j.agrformet.2018.05.016
Rocha, A. D., Vulova, S., Meier, F., Förster, M., & Kleinschmit, B. (2022). Mapping evapotranspirative and radiative cooling services in an urban environment. *Sustainable Cities and Society*, *85*, 104051. https://doi.org/10.1016/j.scs.2022.104051
Rutter, A., Morton, A., & Robins, P. (1975). A predictive model of rainfall interception in forests. II. Generalization of the model and comparison with observations in some coniferous and hardwood stands. *Journal of Applied Ecology*, *12*(1), 367–380. https://doi.org/10.2307/2401739
Salmond, J., Roth, M., Oke, T., Christen, A., & Voogt, J. (2012). Can surface-cover tiles be summed to give neighborhood fluxes in cities? *Journal of Applied Meteorology and Climatology*, *51*(1), 133–149. https://doi.org/10.1175/jamc-d-11-078.1
Scherer, D., Ament, F., Emeis, S., Fehrenbach, U., Leitl, B., Scherber, K., et al. (2019). Three-dimensional observation of atmospheric processes in cities. *Meteorologische Zeitschrift*, *28*(2), 121–138. https://doi.org/10.1127/metz/2019/0911
Schmid, H., & Oke, T. (1990). A model to estimate the source area contributing to turbulent exchange in the surface layer over patchy terrain. *Quarterly Journal of the Royal Meteorological Society*, *116*(494), 965–988. https://doi.org/10.1256/smsqj.49408
Schuepp, P., Leclerc, M., MacPherson, J., & Desjardins, R. (1990). Footprint prediction of scalar fluxes from analytical solutions of the diffusion equation. *Boundary-Layer Meteorology*, *50*(1–4), 355–373. https://doi.org/10.1007/bf00120530
Senate Department for the Environment, Mobility, Consumer and Climate Protection Berlin. (2014). Straßenbefahrung 2014—[WMS] [Dataset]. Retrieved from https://daten.berlin.de/datensaetze/strassenbefahrung-2014-wms-d4c0abae
Senate Department for Urban Development, Building and Housing. (2012). Building and vegetation heights 2012 [Dataset]. Retrieved from https://www.berlin.de/umweltatlas/en/land-use/building-heights/2012/summary
Senate Department for Urban Development, Building and Housing. (2013). Biotope types 2013 [Dataset]. Retrieved from https://www.berlin.de/umweltatlas/en/biotopes/biotope-types/continually-updated/summary/
Solcerova, A., Van de Ven, F., & Van de Giesen, N. (2019). Nighttime cooling of an urban pond. *Frontiers of Earth Science*, *7*, 156. https://doi.org/10.3389/feart.2019.00156
Stagakis, S., Chrysoulakis, N., Spyridakis, N., Feigenwinter, C., & Vogt, R. (2019). Eddy covariance measurements and source partitioning of CO_2 emissions in an urban environment: Application for Heraklion, Greece. *Atmospheric Environment*, *201*, 278–292. https://doi.org/10.1016/j.atmosenv.2019.01.009
Steeneveld, G. J., Koopmans, S., Heusinkveld, B. G., & Theeuwes, N. E. (2014). Refreshing the role of open water surfaces on mitigating the maximum urban heat island effect. *Landscape and Urban Planning*, *121*, 92–96. https://doi.org/10.1016/j.landurbplan.2013.09.001
Teuling, A. J., Seneviratne, S. I., Stöckli, R., Reichstein, M., Moors, E., Ciais, P., et al. (2010). Contrasting response of European forest and grassland energy exchange to heatwaves. *Nature Geoscience*, *3*(10), 722–727. https://doi.org/10.1038/ngeo950
Teuling, A. J., Seneviratne, S. I., Williams, C., & Troch, P. (2006). Observed timescales of evapotranspiration response to soil moisture. *Geophysical Research Letters*, *33*(23), L23403. https://doi.org/10.1029/2006gl028178
Theeuwes, N. E., Solcerova, A., & Steeneveld, G. J. (2013). Modeling the influence of open water surfaces on the summertime temperature and thermal comfort in the city. *Journal of Geophysical Research: Atmospheres*, *118*(16), 8881–8896. https://doi.org/10.1002/jgrd.50704
Valente, F., David, J., & Gash, J. (1997). Modelling interception loss for two sparse eucalypt and pine forests in central Portugal using reformulated Rutter and Gash analytical models. *Journal of Hydrology*, *190*(1–2), 141–162. https://doi.org/10.1016/s0022-1694(96)03066-1
van Dijke, A. J. H., Orth, R., Teuling, A. J., Herold, M., Schlerf, M., Migliavacca, M., et al. (2023). Comparing forest and grassland drought responses inferred from eddy covariance and Earth observation. *Agricultural and Forest Meteorology*, *341*, 109635. https://doi.org/10.1016/j.agrformet.2023.109635
Velasco, E., Pressley, S., Grivicke, R., Allwine, E., Coons, T., Foster, W., et al. (2009). Eddy covariance flux measurements of pollutant gases in urban Mexico City. *Atmospheric Chemistry and Physics*, *9*(19), 7325–7342. https://doi.org/10.5194/acp-9-7325-2009
Vesala, T., Kljun, N., Rannik, Ü., Rinne, J., Sogachev, A., Markkanen, T., et al. (2008). Flux and concentration footprint modelling: State of the art. *Environmental Pollution*, *152*(3), 653–666. https://doi.org/10.1016/j.envpol.2007.06.070
Vulova, S., Kuhlemann, L.-M., Tetzlaff, D., Soulsby, C., & Kleinschmit, B. (2019). Assessment of evapotranspiration from urban vegetation across space and time: A case study in Berlin. In *2019 10th international workshop on the analysis of multitemporal remote sensing images (multitemp)* (pp. 1–4).
Vulova, S., Meier, F., Rocha, A. D., Quanz, J., Nouri, H., & Kleinschmit, B. (2021). Modeling urban evapotranspiration using remote sensing, flux footprints, and artificial intelligence. *The Science of the Total Environment*, *786*, 147293. https://doi.org/10.1016/j.scitotenv.2021.147293
Vulova, S., Rocha, A. D., Meier, F., Nouri, H., Schulz, C., Soulsby, C., et al. (2023). City-wide, high-resolution mapping of evapotranspiration to guide climate-resilient planning. *Remote Sensing of Environment*, *287*, 113487. https://doi.org/10.1016/j.rse.2023.113487
Wang, W., & Davis, K. J. (2008). A numerical study of the influence of a clearcut on eddy-covariance fluxes of CO_2 measured above a forest. *Agricultural and Forest Meteorology*, *148*(10), 1488–1500. https://doi.org/10.1016/j.agrformet.2008.05.009
Wang, W., & Shu, J. (2020). Urban renewal can mitigate urban heat islands. *Geophysical Research Letters*, *47*(6), e2019GL085948. https://doi.org/10.1029/2019gl085948
Ward, H., & Grimmond, C. (2017). Assessing the impact of changes in surface cover, human behaviour and climate on energy partitioning across greater London. *Landscape and Urban Planning*, *165*, 142–161. https://doi.org/10.1016/j.landurbplan.2017.04.001

Wouters, H., Demuzere, M., De Ridder, K., & van Lipzig, N. P. (2015). The impact of impervious water-storage parametrization on urban climate modelling. *Urban Climate*, *11*, 24–50. https://doi.org/10.1016/j.uclim.2014.11.005

Wu, K., Davis, K. J., Miles, N. L., Richardson, S. J., Lauvaux, T., Sarmiento, D. P., et al. (2022). Source decomposition of eddy-covariance CO_2 flux measurements for evaluating a high-resolution urban CO_2 emissions inventory. *Environmental Research Letters*, *17*(7), 074035. https://doi.org/10.1088/1748-9326/ac7c29

Xiao, Q., & McPherson, E. G. (2011). Rainfall interception of three trees in Oakland, California. *Urban Ecosystems*, *14*(4), 755–769. https://doi.org/10.1007/s11252-011-0192-5

Zeeman, M., Benjamins, K., Briegel, F., Drouin, M.-A., Feigel, G., Fenner, D., et al. (2023). A modular data management approach for environmental observation campaigns in multiple cities (Tech. Rep.). *Copernicus Meetings*.

Zimmermann, F., Köstler, H., Grabowski, C., Moeck, M., Saure, C., & Kielhorn, K.-H. (2015). Beschreibung der biotoptypen.